EEET ECOLOGICAL ENGINEERING & ENVIRONMENTAL TECHNOLOGY

Ecological Engineering & Environmental Technology, 2026, 27(5), 399–412
https://doi.org/10.12912/27197050/220341
ISSN 2719–7050, License CC-BY 4.0

Received: 2026.03.18
Accepted: 2026.04.15
Published: 2026.05.01

Urban sprawl, drainage inadequacy, and flood risk co-production in a semi-arid Algerian city: A diachronic geospatial and remote-sensing analysis of Khenchela (1985–2035)

Daoud Zeroual[1*], Islam Boukhelkhal[2], Benchenna Abdelali[3], Ibtissem Lounis[1]

[1] Department of Architecture, Faculty of Sciences and Technology, Chahid Cheikh Elaarbi Tebessi University, 12000 Tébessa, Algeria
[2] Department of Architecture, Faculty of Architecture and Urbanism, Constantine 3 University, 25000 Constantine, Algeria
[3] Department of Architecture, Faculty of Sciences and Technology, University of Jijel, 18000 Jijel, Algeria
* Corresponding author's e-mail: daoud.zeroual@univ-tebessa.dz

ABSTRACT

Khenchela, a medium-sized Algerian city situated in the semi-arid Aurès massif (Eastern Algeria, North Africa), exemplifies a growing class of rapidly urbanising cities where flood risk results less from climatic extremes per se than from the cumulative interaction of uncontrolled urban expansion, ageing drainage infrastructure, and the systematic exclusion of hydrological constraints from urban planning. This study investigates the co-production of flood vulnerability in the inter-municipal grouping of Khenchela through an integrated diachronic framework combining multi-temporal Landsat remote sensing (1985–2025), GIS-based morpho-hydrological analysis, and technical diagnosis of a 265.5 km combined sewer network. Two structurally coupled mechanisms are identified. The first is a morphological dimension characterised by a fourfold increase in built-up surface at the municipal scale (3.48 → 14.10 km²) and a more than five-fold increase at the inter-municipal scale (4.20 → 21.81 km²), progressive colonisation of natural drainage corridors, and transition from a compact radio-concentric urban form to a fragmented polycentric configuration. The second is a technical dimension embodied by a combined sewer system dimensioned for a 1998 urban perimeter, now structurally inadequate relative to current hydrological loads, as reflected by a runoff coefficient increase from C = 0.46 to C = 0.55. Field validation of 22 documented overflow points confirms 87% spatial concordance with modelled conflict zones. A CA-ANN prospective simulation (MOLUSCE/QGIS, κh = 0.87) projects a built-up surface of 28–30 km² by 2035, with a runoff coefficient exceeding 0.62 and peak discharge increases of 40–60% under RCP 4.5. The fully open-source, reproducible, and scalable methodological framework is directly applicable to comparable medium-sized cities in semi-arid North Africa and the Global South facing similar urbanization-infrastructure mismatches.

Keywords: Algeria, North Africa, medium-sized city, urban sprawl, land use/land cover change, flood risk co-production, stormwater infrastructure, cellular automata-artificial neural network simulation, integrated urban resilience.

INTRODUCTION

Global and regional context: urban flooding as a socio-spatial construction

Flood risk in urbanising cities is increasingly recognised as a socio-spatial construction rather than a purely natural phenomenon (Rentschler et al., 2022; Pelling and Garschagen, 2019). Between 1990 and 2020, floods accounted for over 50% of all natural disasters globally, and their frequency and severity are projected to intensify under combined climate change and urbanisation trajectories (Avila-Aceves et al., 2023). In arid and semi-arid regions-where rapid urban growth intersects with limited drainage infrastructure and data-scarce hydrological environments- the threat is particularly acute (Chakrabortty et al., 2025; Hassan et al., 2022). Urban expansion generates a progressive reduction in pervious surfaces, perturbs evapotranspiration, hinders groundwater recharge, and

accumulates surface runoff, substantially amplifying flood risk (Ferreira et al., 2022). Empirical evidence from fast-growing cities in the MENA region consistently shows that peak discharge increases are driven primarily by land-use change rather than by climate variability alone (Gu and Tang, 2023; Anuthaman et al., 2023).

In North Africa, this problem takes a structurally specific form. Flash floods have become the dominant natural hazard across the region, with recent severe events documented in Morocco, Tunisia, Libya, and repeatedly in Algeria (Hadiani et al., 2020; Salhi et al., 2024). Semi-arid wadi systems characterised by intermittent regimes, steep upstream catchments, and bimodal precipitation generate intense short-duration flows converging on downstream urban centres whose stormwater infrastructure was designed for far smaller populations and lower imperviousness (Hadiani et al., 2020). The intersection of these physical dynamics with uncontrolled peri-urban sprawl, deteriorating sewer networks, and weak inter-municipal governance constitutes a systemic vulnerability whose spatial signature is readily detectable through remote sensing and GIS-based morpho-hydrological analysis (Sun et al, 2022; Saidi et al, 2023).

Algeria represents a particularly instructive national context. Its urban population grew from 31% (1966) to over 73% (2023) (Saidi et al, 2023). Studies on Algiers (Keraghel and Gaouaou, 2025), Skikda (Leulmi et al., 2023), and the Mitidja plain (Bengherbia et al., 2025) converge on a common finding: the expansion of impervious surfaces under urbanisation increases surface runoff by 30–50%, progressively exceeding the hydraulic capacity of combined sewer systems designed for earlier urban configurations (Lounis et al., 2024; Abbas, 2024).

Research gap and positioning

The scientific literature on urban flood vulnerability in semi-arid cities has advanced considerably since 2020. Rentschler et al., (2022) established that over one billion people worldwide are exposed to flood hazard, with the largest concentrations in rapidly urbanising cities of the Global South, where climate-related disasters disproportionately threaten the most vulnerable urban populations (Hallegatte et al., 2017). Chakrabortty et al., (2025) demonstrated that impervious surface expansion and inadequate stormwater infrastructure are the primary structural drivers of flood susceptibility. Salhi et al, (2024) showed how informal urban expansion and deteriorating drainage produce flood episodes that are environmental and psychosocial in equal measure. Hassan et al., (2022) confirmed, for New Cairo (Egypt), that drainage design inadequacy is the dominant risk amplifier in arid contexts. Despite this growing body of evidence, no study has systematically analysed flood vulnerability in the inter-municipal grouping of Khenchela-a mid-sized wilaya capital characterised by an exceptionally rapid urbanisation trajectory (+419% built-up surface between 1985 and 2025). The existing literature has predominantly focused on coastal or metropolitan contexts, leaving the semi-arid interior underrepresented. This study addresses these gaps.

Research questions, hypothesis, and objectives

The central research question is: How has the synergy between uncontrolled urban expansion and structurally inadequate sewer infrastructure progressively co-produced flood vulnerability in Khenchela over four decades (1985–2025), and what integrated spatial risk indicators can be derived for the 2035 horizon? We posit a dual flood risk co-production mechanism: (i) a morphological dimension driven by urban sprawl and colonisation of drainage corridors; and (ii) a technical dimension embodied by a combined sewer system dimensioned for 1998 conditions, now structurally mismatched to current hydrological loads. Four operational objectives are pursued: (i) reconstruct LULC and morphological dynamics (1985–2025); (ii) characterise morpho-hydrological conflict zones; (iii) diagnose sewer network structural inadequacy; and (iv) simulate urban expansion and flood risk intensification to 2035.

STUDY AREA

The study area encompasses the inter-municipal grouping of Khenchela, comprising three functionally integrated localities: the city of Khenchela (32 km², wilaya capital since 1984), El Hamma (216.95 km², 8 km north-west), and Ensigha (214.84 km², south-east), covering a total administrative area of 463.79 km² (Table 1; Figure 1). The inter-municipal master plan (PDAU 2023) formally integrates these three localities into a single urban planning unit. Population in 2025 is

estimated at 175,800 inhabitants, with Khenchela absorbing the dominant share (145,000) due to its administrative status (DPSB, 2025).

Khenchela is established at 1.100–1.200 m A.S.L. within the Aurès massif (Figure 2). Its hydrological position is structurally exposed: the Bougheoul wadi (catchment: 74.26 km², 14 sub-basins, torrential regime) collects run-off from the northern mountainous sector and drains through the expanding urban fabric toward downstream accumulation zones. Slopes exceeding 18% cover over 70% of upstream surfaces, generating short concentration times and high peak discharges. The bioclimate is semi-arid to sub-humid montane Mediterranean, with mean annual precipitation of 380 mm and a bimodal seasonal regime characterised by autumn and spring peaks, with hourly intensities exceeding 40 mm/h during convective events (Figure 3) (Station Météo Algérie, 2023).

Table 1. Territorial distribution of the study area

Municipality	Area (km²)	Population 2025
Khenchela	32.00	145,000
El Hamma	216.95	18,500
Ensigha	214.84	12,300
Total	463.79	175,800

Note: DPSB (2025).
Total administrative area: 463.79 km².

MATERIALS AND METHODS

Satellite data and pre-processing

A Landsat time series covering five acquisition dates (1985, 1995, 2005, 2015, 2025) was assembled from USGS Earth Explorer (Level L1TP). Landsat 5 TM scenes (path 192, rows 034–035) were used for 1985, 1995, and 2005; Landsat 8 OLI/TIRS for 2015 and 2025. Acquisitions were made during the dry season (May–August). All scenes present cloud cover below 0.1%. Geometric accuracy was confirmed at RMSE ≤ 0.26 pixel in WGS84, UTM Zone 32N. Pre-processing followed a standard chain: TOA reflectance conversion, atmospheric correction (DOS1), and false-colour compositing (bands 4-3-2 for TM; 5-4-3 for OLI-TIRS) (Fichera et al., 2012; Wulder et al., 2022).

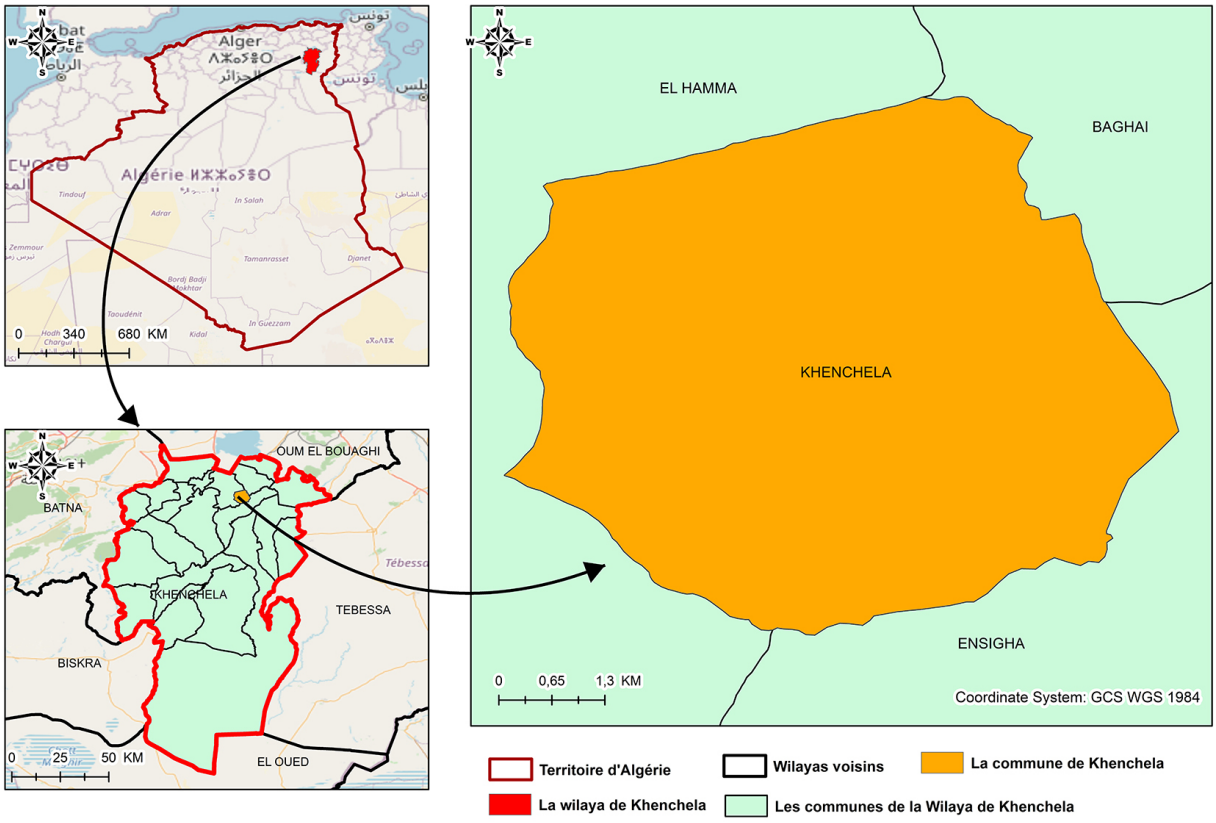

Figure 1. Administrative map of the Khenchela inter-municipal grouping and secondary localities.
Source: DPSB (2025)

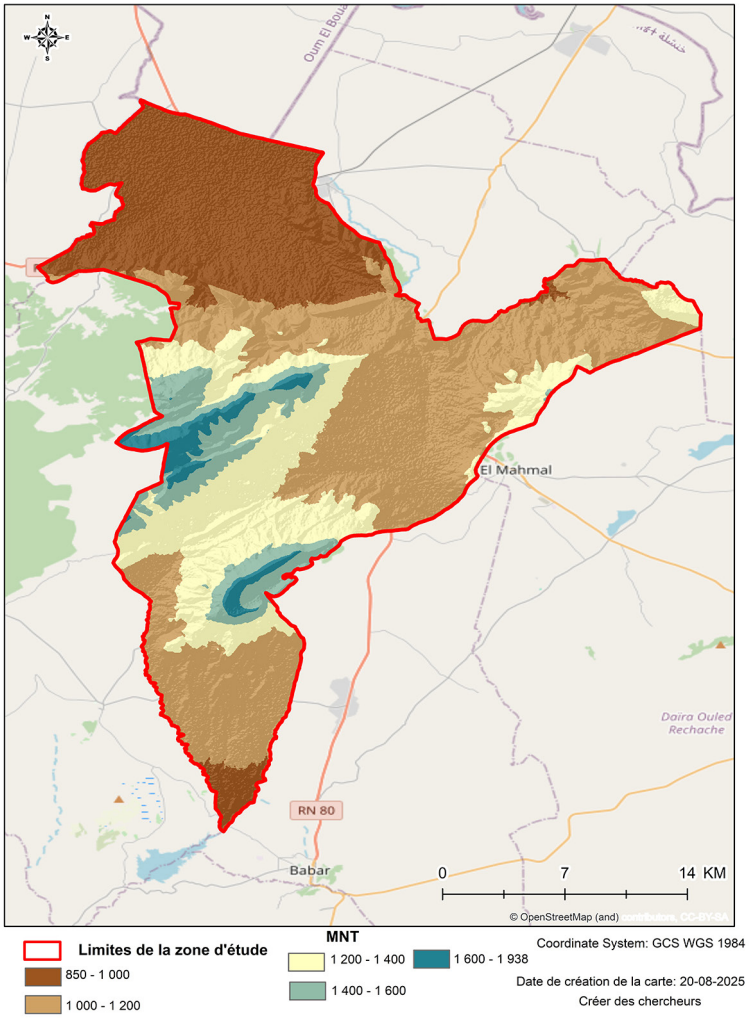

Figure 2. Topography and relief of the Khenchela region. Source: DPSB (2025)

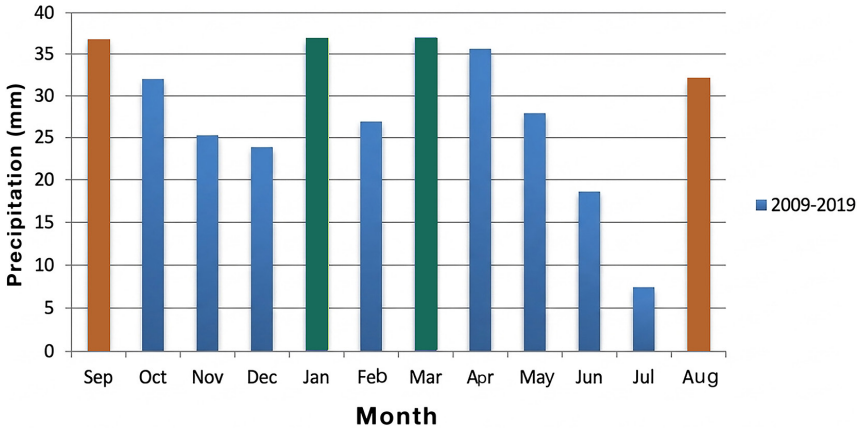

Figure 3. Average monthly rainfall in Khenchela (bimodal regime). Source: Station Météo Algérie (2024)

Land-use/land-cover classification and accuracy assessment

Four LULC classes were retained as defined in Table 2: Built-up surfaces, Vegetation, Forest, and Bare/arid land. Classification was performed using the Random Forest (RF) algorithm (ntree = 500, QGIS Orfeo ToolBox), selected for its documented superiority in semi-arid environments (Wang et al., 2022). A minimum of 80 stratified random training samples per class per date were

Table 2. Land-use/land-cover classes used for classification and their associated runoff coefficients

Class	Description	Runoff Coeff. (C)
Built-up	Impermeable surfaces, residential areas, and human settlements	0.75
Vegetation	Dense vegetative cover	0.20
Arid lands	Bare soils or sparse vegetative cover	0.40
Forests	Wooded formations	0.15

Note: Runoff coefficients (C) are class-specific values used in the weighted runoff calculation (Equation 1).

collected (320 total per date). Accuracy assessment yielded overall accuracy (OA) from 88.5% to 93.7% and Kappa coefficients (κ) from 0.84 to 0.91 across all five dates.

Diachronic morphological and hydrological analysis

Diachronic LULC maps were analysed in a GIS framework to quantify class-level area changes and transition matrices at each interval. The hydrographic network, sub-basin delineation, and watershed slope distribution are presented in Figures 7 and 8. The runoff coefficient (C) for each date was estimated through a dual weighted-empirical approach. The area-weighted mean was calculated as shown in Equation 1:

$$C = \Sigma(C_n \times S_i / S\_total) \quad (1)$$

where: C_n is the class-specific runoff coefficient (Table 2), S_i the surface area of class *i*, and *S_total* the total study area.

This was cross-validated against the empirical correction proposed by Arnell (1999):

$$C = 0.14 + 0.65U + 0.05P \quad (2)$$

where: *U* is the imperviousness ratio and *P* the mean catchment slope (*P* = 0.055 for 5.5%).

Urbanisation maps were intersected with the SRTM 30 m DEM and hydrographic network to identify morpho-hydrological conflict zones, following the spatial assessment framework proposed by Nedelea et al. (2020). Conflict zone accuracy was validated against 22 georeferenced overflow points documented during the November 2023 and September 2024 flood episodes, yielding 87% spatial concordance.

Technical diagnosis of the sewer network

Sewer network data were obtained from the Direction des Ressources en Eau (DRE, 2021) and STEP Khenchela (2025). The diagnosis characterised network type, total length (265.5km), connection rate, and outfall configuration (Table6). Structural inadequacy was assessed by comparing 1998 PDAU design parameters (≈60,000 inhabitants, C = 0.46) against current conditions (≈154,000 inhabitants, C = 0.55) and projected 2035 loads. Hydraulic dysfunctions were mapped at the 22 critical points using 1:25,000 topographic data and DRE field records.

CA-ANN prospective simulation (2025–2035)

Prospective urban expansion was simulated using the CA-ANN framework (MOLUSCE plugin, QGIS), trained on the 2015–2025 LULC transition matrix with five spatial driver variables: distance to roads, distance to existing built-up areas, slope, altitude, and population density. These five variables were selected based on their established predictive significance in the semi-arid urban growth literature (Muhammad et al., 2022; Lukas et al., 2023) and their documented role as primary drivers of built-up expansion in topographically constrained Algerian cities (Guechi and Alkama, 2017). Model performance was validated against the actual 2025 classification, yielding κh = 0.87. The BAU scenario was projected to 2035, integrating RCP 4.5 precipitation projections (Bibi and Kara, 2023; Islam et al., 2025).

RESULTS

LULC dynamics and spatial polarisation (1985–2025)

The five-date LULC analysis illustrated in Figure 4 reveals a dramatic transformation of the regional land surface. At the Khenchela municipal scale (Table 3), built-up surfaces quadrupled from 3.48 km² (11.04%) in 1985 to 14.10 km² (44.75%) in 2025 (+305.2%). At the inter-municipal scale (Table 4), the increase was 4.20 km² to 21.81 km²,

a 419.3% growth driven by a rapid expansion phase (1985–2005, +273%, CAGR +2.8%) and a consolidation phase (2005–2025, +39%, CAGR +1.7%). Bare/arid land declined from 339.07 km² to 321.72 km², while forest cover decreased by 3.1%. The runoff coefficient increased from C = 0.46 (1985) to C = 0.55 (2025), a 19.6% amplification of surface runoff generation capacity.

Population density by municipality is illustrated in Figure 5. Khenchela municipality concentrated over 80% of regional urbanisation. El Hamma and Ensigha registered proportionally high growth rates from near-zero baselines (+1.615% and +1.026% respectively) but their combined built-up surfaces represent less than 18% of the regional total in 2025.

Urban morphological transition and hydrological implications

The diachronic analysis documents a fundamental morphological transition illustrated in Figure 6. Until 2005, Khenchela's expansion followed a predominantly radio-concentric model anchored on the colonial core (~2 km²). From 2005 onward, three concurrent tendencies define the emerging fragmented polycentric configuration: (i) preferential alignment of built fabric along national roads RN 80, 88, and 32; (ii) multiplication of secondary poles (university campus, industrial zone, new housing estates); and (iii) diffuse development generating spatial discontinuities. This ribbon development pattern interrupts transverse hydraulic trajectories, encroaches on natural drainage corridors, and multiplies the interface between impermeable surfaces and overflow-prone zones (Leulmi et al., 2023; Guechi and Alkama, 2017).

The intersection of urbanisation maps with the SRTM 30 m DEM and hydrographic network (Figure 7) identifies 22 critical morpho-hydrological conflict points (Figure 8) distributed across three priority risk sectors: (i) the northern sector, subject to direct Bougheoul wadi and Chabord hill runoff contribution; (ii) the eastern sector at ~1.060 m, where thalweg culverting has broken natural hydraulic continuity; and (iii) the southern sector, comprising low-lying downstream receptor zones subject to sewer backflow (Figure 9). The spatial concordance rate between modelled conflict zones and field-documented overflow points is 87%.

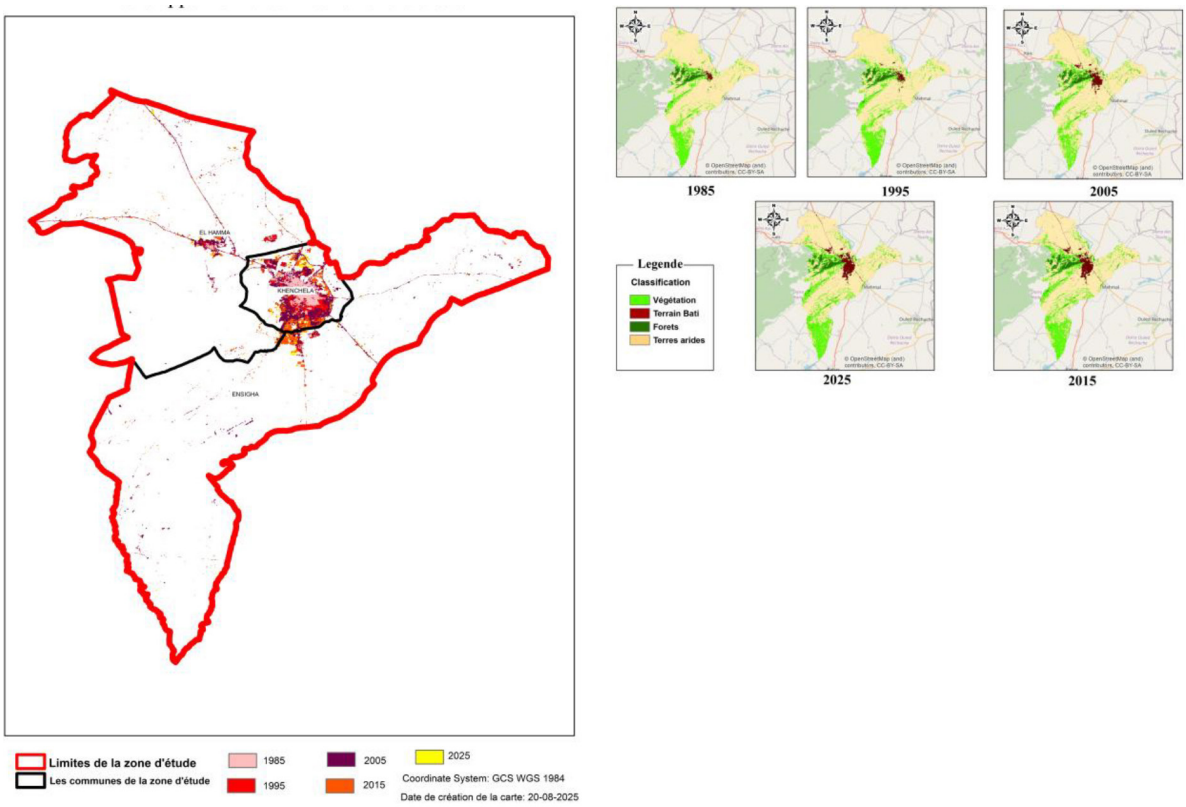

Figure 4. Multi-temporal Landsat satellite imagery of the Khenchela region (representative dates 1985, 1995, 2005, 2015, 2025 with overlay map)

Table 3. Land-use/land-cover change in the city of Khenchela (1985–2025)

Class	1985 (km²)	1985 (%)	2025 (km²)	2025 (%)	Var. (%)	AAGR (%/yr)
Built-up	3.48	11.04	14.10	44.75	+305.2	+2.05
Vegetation	9.82	31.15	8.45	26.81	−13.9	−0.39
Arid lands	16.20	51.41	8.26	26.21	−49.0	−0.79
Forests	1.98	6.28	0.71	2.25	−64.1	−2.25

Note: AAGR: Annual Average Growth Rate = [(Area-2025/Area-1985)^(1/40) - 1] × 100.

Table 4. Land-use/land-cover change at the inter-municipal grouping level (1985–2025).

Class	1985 (km²)	1985 (%)	2025 (km²)	2025 (%)	Var. (%)	AAGR (%/yr)
Built-up	4.20	1.31	21.81	4.70	+419.3	+2.32
Vegetation	99.54	21.45	103.62	22.34	+4.1	+0.10
Arid lands	339.07	73.09	321.72	69.37	−5.1	−0.13
Forests	18.23	3.93	17.66	3.81	−3.1	−0.08

Note: El Hamma registered +1.615% and Ensigha +1.026% built-up growth from near-zero 1985 baselines.

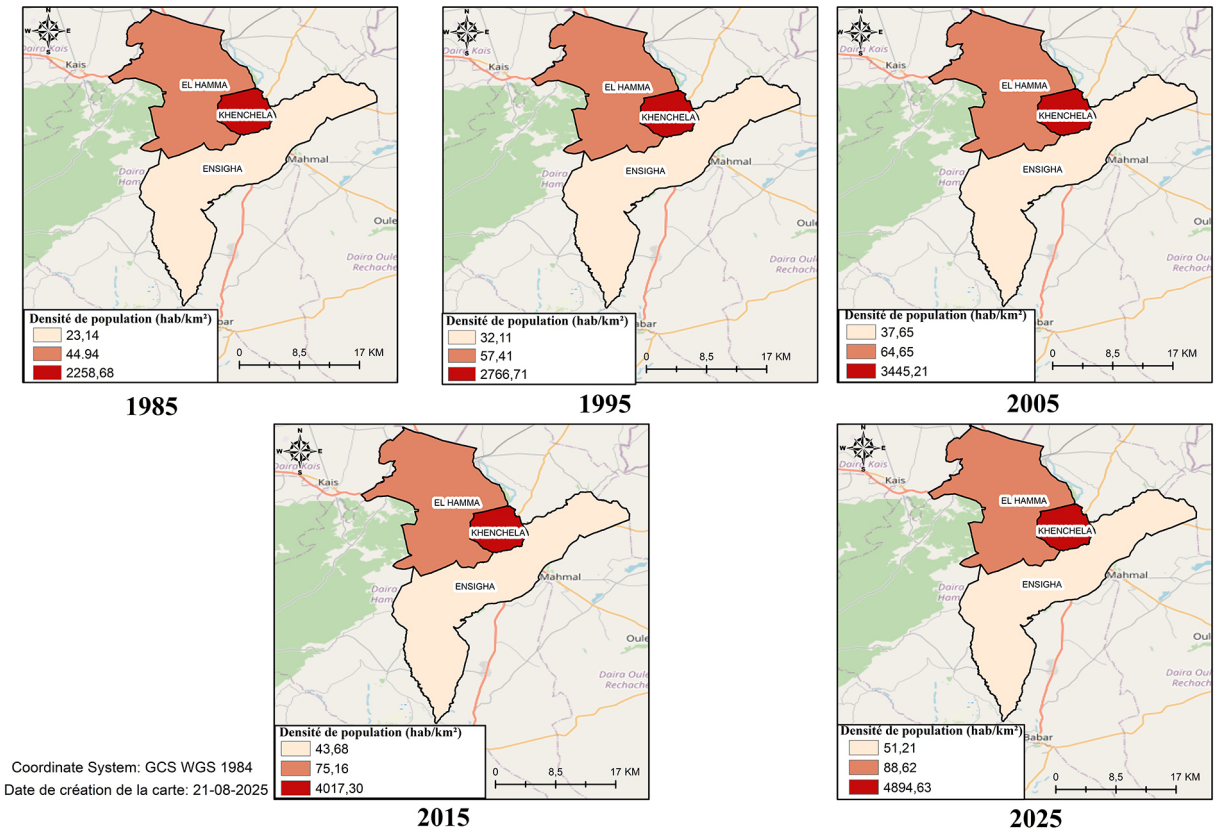

Figure 5. Choropleth map of population density by municipality across the inter-municipal grouping (1985–2025)

Runoff amplification: from measured imperviousness to quantified risk

The dual runoff coefficient estimation (Table 5) confirms the structural amplification of hydraulic loads through urbanisation. The area-weighted mean coefficient C, computed from Equations 1 and 2, increased from 0.46 (1985) to 0.55 (2025), driven primarily by the explosion of built-up surface whose weighted runoff contribution grew from 0.026 to 0.106. A coefficient exceeding 0.50 signals elevated hydraulic vulnerability. Projected 2035 conditions (C ≈ 0.62–0.68 under BAU) would push the system decisively beyond the

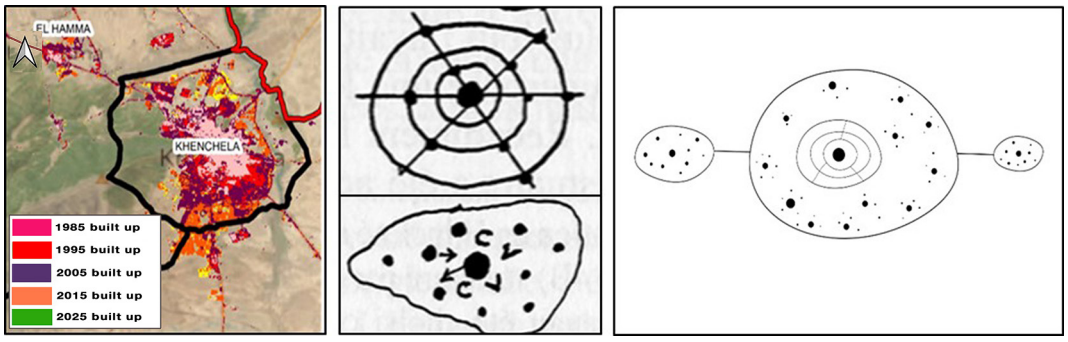

Figure 6. Urban development model: transition from radio-concentric to fragmented polycentric configuration (1985–2035)

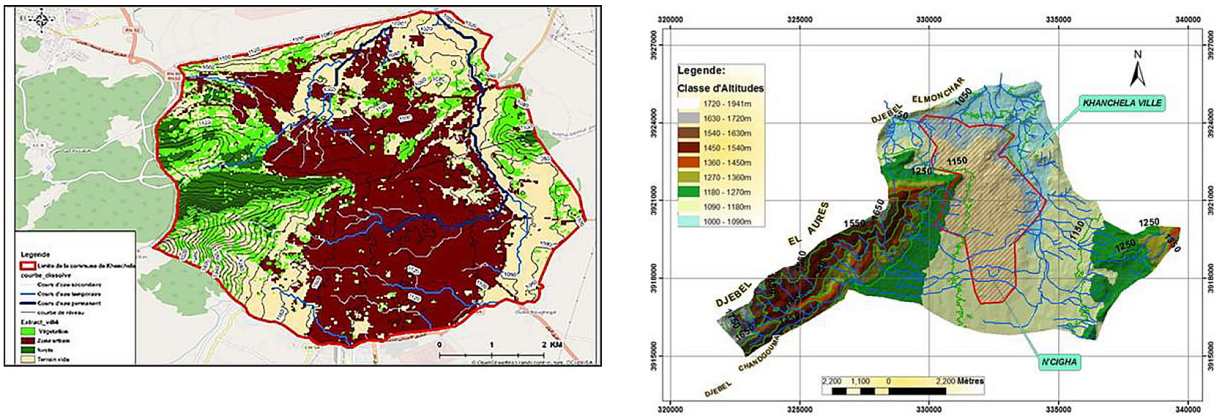

Figure 7. Cross-referenced DTM-hydromorphology-land use (left) and slope classes with rapid runoff potential (right) in the Bougheoul wadi watershed (Khenchela)

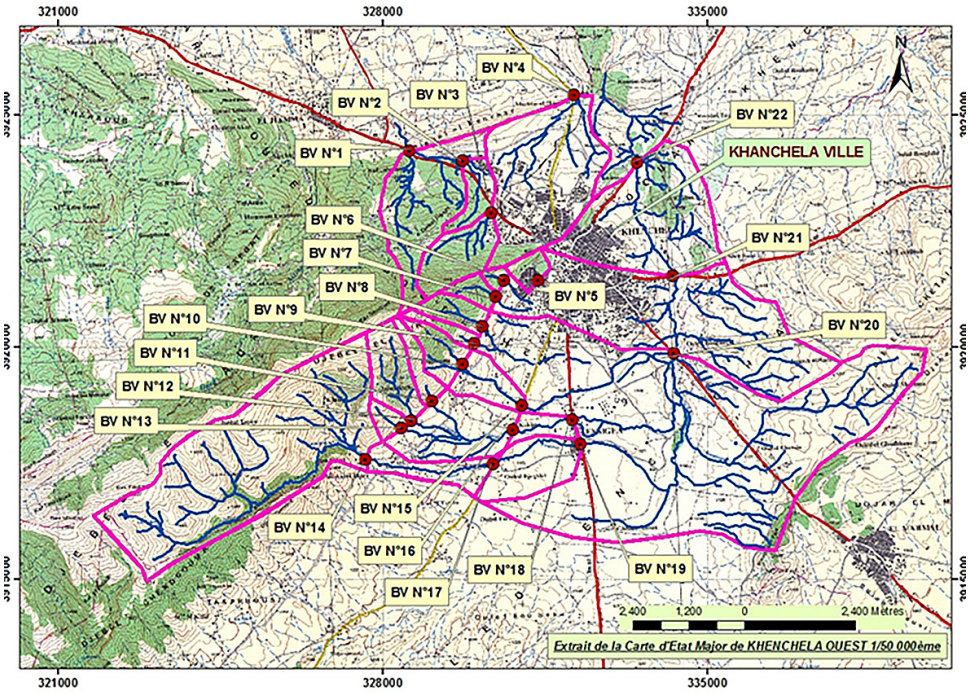

Figure 8. Hydrographic network and sub-basins draining the city of Khenchela (network overlay; sub-basin delineation)

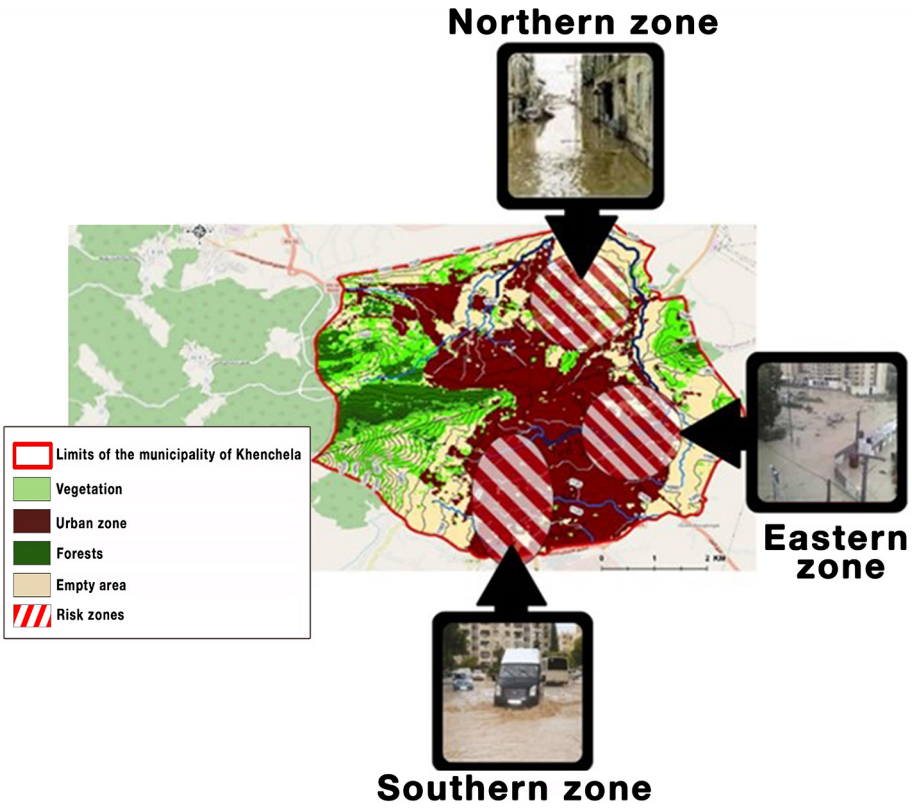

Figure 9. Conflict-risk zones in the northern, eastern, and southern sectors of Khenchela

Table 5. Urban runoff coefficient by land-use class in Khenchela municipality (1985–2025)

Class	C	1985 Area (km²)	1985 C×S	2025 Area (km²)	2025 C×S	Δ Contribution
Built-up	0.75	3.48	0.026	14.10	0.106	+0.080
Vegetation	0.20	9.82	0.020	8.45	0.017	−0.003
Arid lands	0.40	16.20	0.065	8.26	0.033	−0.032
Forests	0.15	1.98	0.003	0.71	0.001	−0.002
Total area	—	31.48	—	31.52	—	—
Global C	—	—	0.46	—	0.55	+19.6%

Note: C×S is the area-weighted runoff contribution per class ($C_n \times S_i/S\_total$ per Equation 1).
The built-up class accounts for the dominant share of global C amplification (+0.080 units, 1985–2025).

hydraulic envelope of any presently feasible infrastructure upgrade.

Sewer network diagnosis: structural inadequacy as risk co-producer

The combined sewer network of Khenchela (265.5 km) was dimensioned under the 1998 PDAU for approximately 60,000 inhabitants with C = 0.46. Current conditions have fundamentally invalidated these parameters: population has reached approximately 154,000 (2025), C has risen to 0.55, and the urbanised area has more than quadrupled. The structural diagnosis is summarised in Table 6. Three hydraulic dysfunctions are documented: (i) pipe surcharging during intense precipitation; (ii) manhole overflow and backflow in topographically low sectors; and (iii) unregulated discharge of mixed effluents directly into the Bougheoul wadi (Figure 10), transferring hydraulic risk to downstream urban areas (Kirk et al., 2024).

The 22 field-documented overflow points cluster in the three morphologically identified risk sectors, confirming that hydraulic failure occurs precisely at the intersection of maximum imperviousness, topographic convergence, and network under-dimensioning. This spatial co-localisation validates the integrated diagnostic approach and

Table 6. Summary diagnosis of the Khenchela combined sewer network.

Characteristic	Diagnosis	Impact on flood risk
Network type	Predominantly combined sewer (wastewater + stormwater)	Rapid saturation during heavy rainfall events
Total length	265.5 km	Insufficient for current urbanised area and hydraulic loads
Connection rate	Not fully quantified in field diagnosis	Unconnected sectors generating uncontrolled diffuse runoff
Final outlet	Direct discharge into Oued Bougheoul without treatment or regulation	Risk transferred to urbanised riverbanks and downstream sectors
General condition	Dilapidated, partially obstructed; insufficient maintenance	Reduced hydraulic capacity relative to nominal design
Design basis	Based on 1998 PDAU for a much smaller urban fabric (≈60,000 inh.)	Structurally undersized for 2025 and 2035 conditions

Note: DRE (2021); STEP Khenchela (2025); Authors (2025). Network length revised to 265.5 km following 2021 DRE field audit.

Figure 10. Direct discharge of excess stormwater into the Bougheoul wadi at the urban fringe, documenting the unregulated outfall configuration of the combined sewer network. Source: DRE (2021)

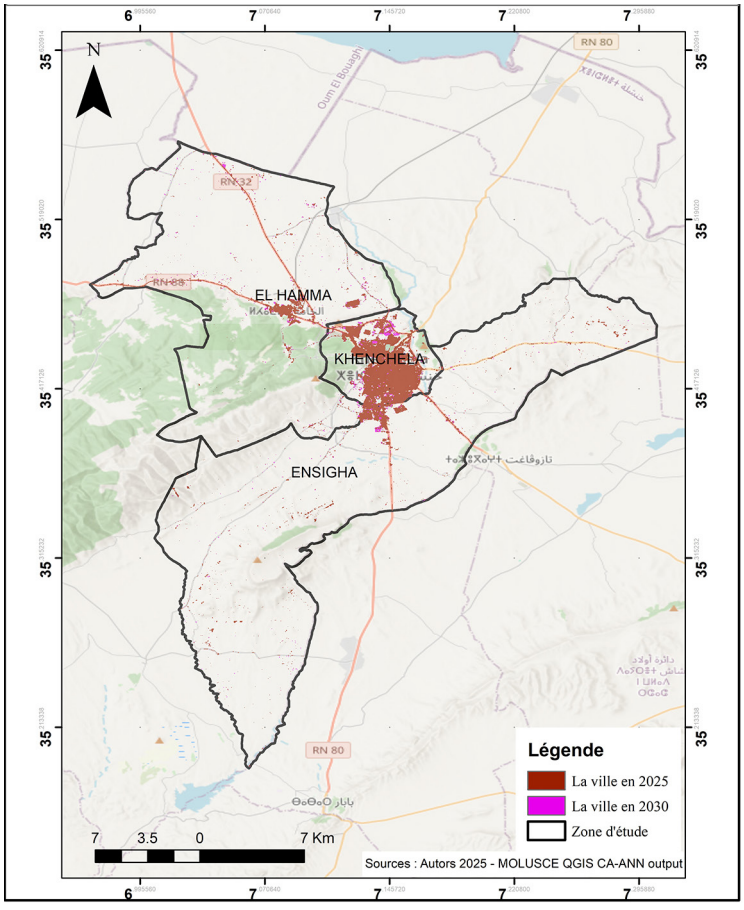

Figure 11. Satellite imagery of the projected urban area in 2035 derived from the CA-ANN/MOLUSCE BAU simulation (κh = 0.87)

demonstrates that the sewer network operates as an active co-producer of urban flood vulnerability (Kirk et al., 2024).

CA-ANN prospective simulation – 2035 flood risk intensification

The cellular automata–artificial neural network simulation (κh = 0.87) projects, under the BAU scenario, a built-up surface of 28–30 km² by 2035 at the inter-municipal scale, as illustrated in Figure 11. The runoff coefficient is projected to reach C ≈ 0.62–0.68, generating surface flows exceeding the hydraulic capacity of the existing network by factors of 1.4–1.8 at peak events. Integrating RCP 4.5 regional precipitation projections, peak catchment discharges are expected to increase by 40–60% relative to the 2025 baseline (Bibi and Kara, 2023). Three convergent risk trajectories are identified: (i) in-situ densification in the central core; (ii) linear coalescence of secondary localities along road axes; and (iii) progressive encroachment on high-risk southern receptor zones.

DISCUSSION

The dual flood risk co-production mechanism – morphological and technical dimensions

The results confirm and empirically substantiate the central hypothesis of a dual flood risk co-production mechanism. This finding extends the conceptual framework of vulnerability as socio-spatial construction (Reghezza-Zitt and Rufat, 2015), demonstrating that in Khenchela's specific context, risk is an actively produced outcome of urban planning choices and infrastructure management decisions cumulated over four decades. The morphological dimension- characterised by a 419% increase in built-up surfaces (Tables 3–4), progressive colonisation of drainage corridors (Figure 7), and transition from compact to fragmented polycentric form (Figure 6)- generates quantifiable runoff amplification (C: 0.46 → 0.55, Table 5). The 419% built-up growth documented at Khenchela substantially exceeds the 45–68% reported for comparable Algerian cities (Leulmi et al., 2023; Guechi and Alkama, 2017), reflecting the compound effect of administrative promotion to wilaya capital status (1984) and severe topographic constraints.

The technical dimension-embodied by a combined sewer system operating at roughly 2.5 times its design population load with C 19.6% above calibration (Table 6)-constitutes a structurally self-reinforcing vulnerability amplifier. This finding resonates with Keraghel and Gaouaou's (2025) analysis for Algiers and confirms the MENA pattern identified by Hadiani et al., (2020). Critically, the interaction between these two dimensions is not merely additive but multiplicative: morphological fragmentation routes runoff toward hydraulic conflict points precisely where the sewer network is most structurally inadequate. This spatial co-localisation-empirically confirmed by the 87% concordance between modelled conflict zones (Figure 9) and observed overflow points-constitutes the defining characteristic of Khenchela's flood risk co-production system.

Contextualisation within North African and Global South urban dynamics

Khenchela's trajectory finds specific parallels in the literature on medium-sized Global South cities confronted with rapid administrative promotion and constrained planning capacity. The combination of accelerated urbanisation, topographic constraint, and governance deficit mirrors patterns identified by Amponsah et al. (2022) for rapidly urbanising Ghanaian cities, and by Ferreira et al., (2022) for Doha, Qatar (777% urban area growth between 1984 and 2020, generating a 422% runoff increase). Within Algeria, the documented dynamics align with and extend the findings of Keraghel and Gaouaou (2025), Leulmi et al., (2023), and Bengherbia et al., (2025), adding the specific contribution of an inland topographically constrained mountain city whose flood risk dynamics are shaped by wadi torrentialism and bimodal precipitation absent from coastal metropolitan contexts.

Spatial evidence base for integrated urban resilience

The spatial evidence accumulated in this study supports the identification of three complementary intervention axes derived directly from the diagnostic results. First, the 22 georeferenced conflict points (Figure 9) and the three delineated priority risk sectors constitute the empirical foundation for a flood risk prevention plan (PPRI), whose formal incorporation into

the PDAU revision process would operationalise the spatial risk indicators produced here, in alignment with Sendai Framework Priority 4 (UNDRR, 2015; UNEP, 2018). Second, the documented encroachment on natural drainage corridors (Figures 7 and 6) indicates that blue-green infrastructure and morphological restoration represent spatially targeted responses to identified vulnerabilities; nature-based solutions have demonstrated quantifiable flood risk reduction effectiveness in comparable semi-arid Mediterranean contexts (Lafortezza et al., 2018; Doswald et al., 2014). Third, the sewer diagnosis (Table 6; Figure 10) indicates that a risk-prioritised, sectorised programme of network separation-targeting the 22 critical overflow nodes-would address the most structurally constrained points of the hydraulic system (Hadiani et al., 2020; Keraghel and Gaouaou, 2025).

Methodological contributions and scalability

The integrated Landsat-RF-CA-ANN-MOLUSCE-drainage diagnostic chain, entirely based on open data and open-source tools, constitutes a reproducible methodological protocol directly applicable to the large number of Algerian and North African medium-sized cities for which equivalent studies remain absent. The 87% field-validation concordance rate confirms that the modelled conflict zones provide operationally reliable information for planning prioritisation, without requiring expensive hydraulic modelling software or dense sensor networks (Chakrabortty et al., 2025; Muhammad et al., 2022).

Study limitations

The 30 m Landsat spatial resolution constrains detection of fine-grained informal urban development; Sentinel-2 (10 m) integration would improve precision. The sewer network diagnosis relies on partial DRE data without comprehensive hydraulic field measurement, introducing uncertainty in absolute capacity estimates. The cellular automata-artificial neural network simulation adopts a single BAU scenario; multi-scenario testing would enrich the spatial risk evidence base (Muhammad et al., 2022).

CONCLUSIONS

This study has provided the first integrated diachronic and prospective analysis of flood vulnerability co-production in the inter-municipal grouping of Khenchela (Eastern Algeria, 1985–2025). The main empirical findings are as follows: (i) a 419.3% increase in built-up surfaces (4.20 → 21.81 km²) generating a 19.6% amplification of the runoff coefficient (C: 0.46 → 0.55); (ii) a fundamental morphological transition from a compact radio-concentric urban form to a fragmented polycentric configuration, multiplying the interfaces between impervious surfaces and natural drainage corridors; (iii) a combined sewer network designed for 1998 conditions, now structurally inadequate for a city roughly 2.5 times larger; (iv) 22 field-validated morpho-hydrological conflict points confirming 87% concordance between modelled and observed overflow locations; and (v) a CA-ANN 2035 projection (κh = 0.87) indicating built-up surfaces of 28–30 km², C ≈ 0.62–0.68, and peak discharge increases of 40–60% under RCP 4.5.

All four operational objectives of the study were fully achieved: (i) LULC and morphological dynamics reconstructed over 40 years with high classification accuracy (OA: 88.5–93.7%, κ: 0.84–0.91); (ii) 22 morpho-hydrological conflict zones characterised with 87% field-validation concordance; (iii) the structural inadequacy of the combined sewer network quantified against its 1998 design baseline; and (iv) urban expansion to 2035 projected by CA-ANN with strong predictive performance (κh = 0.87). The central hypothesis of a dual flood risk co-production mechanism – driven by the synergistic interaction of uncontrolled morphological sprawl and structural drainage infrastructure inadequacy -is fully confirmed: the progressive increase in the runoff coefficient (C: 0.46 → 0.55) and the systematic spatial co-localisation of modelled conflict zones with the 22 field-documented overflow points demonstrate unambiguously that flood risk in Khenchela is a socio-spatial outcome actively constructed by four decades of urban planning decisions made without hydrological constraints.

The fully open-source Landsat-GIS-CA-ANN-drainage diagnostic methodology constitutes a reproducible, scalable, and cost-effective framework directly applicable to comparable

medium-sized cities in semi-arid North Africa and the Global South facing equivalent urbanization-infrastructure mismatches. The 87% field-validation concordance rate confirms that the integrated morpho-hydrological approach provides operationally reliable spatial risk information without requiring expensive hydraulic modelling software or dense sensor networks.

Three original scientific contributions distinguish this study from the existing literature. First, it provides the first spatially explicit analysis of flood vulnerability in the Khenchela intermunicipal grouping, filling a documented gap in semi-arid Algerian urban hydrology where topographically constrained interior mountain cities remain absent from comparative studies dominated by coastal and metropolitan contexts. Second, it operationalises and empirically validates the dual co-production framework for a wadi-dominated torrential regime with bimodal precipitation – a configuration previously unaddressed in the MENA flood vulnerability literature. Third, it establishes the operational viability of a fully open-source diagnostic chain (Landsat-RF-CA-ANN-drainage) for generating reliable spatial risk intelligence in data-scarce planning environments, advancing the methodological frontier for comparable cities across North Africa and the Global South. Three research axes emerge as priorities: (i) integration of Sentinel-2 imagery (10 m) for fine-grained informal urbanisation dynamics detection; (ii) multi-scenario CA-ANN modelling contrasting the BAU trajectory with integrated planning alternatives incorporating drainage corridor preservation; and (iii) formalisation of the 22 conflict points and three priority risk sectors into a Flood Risk Prevention Plan integrated within the ongoing PDAU revision process, translating the spatial risk indicators produced here into binding planning instruments.

Acknowledgements

The authors sincerely thank the Direction de la Programmation et du Suivi du Budget (DPSB) of Khenchela wilaya for providing administrative and demographic data, and the Direction des Ressources en Eau (DRE) for sewer network technical documentation. Special thanks are due to the University of Tebessa for institutional support, and to the anonymous reviewers for their constructive feedback.

REFERENCES

1. Abbas, S. (2024). Détection des changements et analyse de l'étalement urbain dans la ville de M'sila (Algérie). *International Journal of Innovative Technologies in Social Science, 4*(44). https://doi.org/10.31435/ijitss.4(44).2024.2947 (in French)
2. Amponsah, O., Blija, D. K., Ayambire, R. A., Takyi, S. A., Mensah, H., Braimah, I. (2022). Global urban sprawl containment strategies and their implications for rapidly urbanizing cities in Ghana. *Land Use Policy, 114*, 105979. https://doi.org/10.1016/j.landusepol.2021.105979
3. Anuthaman, S. N., Ramasamy, S., Ramasubbu, B., Lakshminarayanan, B. (2023). Modelling and forecasting of urban flood under changing climate and land use land cover. *Journal of Water and Climate Change, 14*(12), 4314–4335. https://doi.org/10.2166/wcc.2023.431
4. Arnell, N. W. (1999). The effect of climate change on hydrological regimes in Europe: A continental perspective. *Global Environmental Change, 9*(1), 5–23. https://doi.org/10.1016/S0959-3780(98)00015-1
5. Avila-Aceves, E., Plata-Rocha, W., Monjardin-Armenta, S. A., Rangel-Peraza, J. G. (2023). Flood risk in urban areas: Modelling, management and adaptation to climate change. *Hydrology, 9*(3), 50. https://doi.org/10.3390/hydrology9030050
6. Bengherbia, N., Salhi, A., Hamlaoui-Moulai, L. (2025). From urban sprawl to aquifer strain: The hydrological consequences of LULCC in the Mitidja plain, Algeria. *Journal of Hydrology: Regional Studies, 58*. https://doi.org/10.1016/j.ejrh.2025.102050
7. Bibi, T. S., Kara, K. G. (2023). Evaluation of climate change, urbanization, and low-impact development practices on urban flooding. *Heliyon, 9*(1), e12955. https://doi.org/10.1016/j.heliyon.2022.e12955
8. Chakrabortty, R., Ali, T., Abouleish, M., Pal, S. C., Roy, P. (2025). Urban flood susceptibility assessment in arid environment using a novel hybrid deep learning approach. *Earth Systems and Environment.* https://doi.org/10.1007/s41748-025-00503-3
9. Doswald, N., Munroe, R., Roe, D., Giuliani, A., Castelli, I., Stephens, J., Möller, I., Spencer, T., Vira, B., Reid, H. (2014). Effectiveness of ecosystem-based approaches for adaptation. *Climate and Development, 6*(2), 185–201. https://doi.org/10.1080/17565529.2013.867466
10. Ferreira, C. S. S., Walsh, R. P. D., Ferreira, A. J. D. (2022). Exploring urban growth–climate change–flood risk nexus in fast growing cities. *Scientific Reports, 12*, 12265. https://doi.org/10.1038/s41598-022-16259-9
11. Fichera, C. R., Modica, G., Pollino, M. (2012). Land cover classification and change-detection analysis using multi-temporal remote sensed imagery.

European Journal of Remote Sensing, 45(1), 1–18. https://doi.org/10.5721/EuJRS20124501

12. Gu, T., Tang, J. (2023). Urban flood risk differentiation under land use scenario simulation. *iScience, 26*(4), 106479. https://doi.org/10.1016/j.isci.2023.106479
13. Guechi, I., Alkama, D. (2017). Apport de la télédétection pour la cartographie diachronique de l'étalement urbain de l'agglomération de Guelma. *Courrier du Savoir, 24*, 73–80. (in French) https://doi.org/10.33673/csdb.2017.24.73
14. Hadiani, M., Moghadas, M., Soltani, A. (2020). Flood risk management in the Middle East and North Africa (MENA) region. *Urban Water Journal, 17*(5), 455–470. https://doi.org/10.1080/1573062X.2020.1728401
15. Hallegatte, S., Vogt-Schilb, A., Bangalore, M., Rozenberg, J. (2017). Unbreakable: Building the resilience of the poor in the face of natural disasters. *World Bank.* https://doi.org/10.1596/978-1-4648-1003-9
16. Hassan, B. T., Yassine, M., Amin, D. C. (2022). Comparison of urbanization, climate change, and drainage design impacts on urban flashfloods in an arid region. *Water, 14*(15), 2430. https://doi.org/10.3390/w14152430
17. Islam, T., Zeleke, E. B., Afroz, M., Melesse, A. M. (2025). A systematic review of urban flood susceptibility mapping. *Remote Sensing, 17*(3), 524. https://doi.org/10.3390/rs17030524
18. Keraghel, M. A., Gaouaou, F. (2025). Assessing flood dynamics in Algiers, Algeria: Influence of land cover change and precipitation regimes. *Theoretical and Applied Climatology, 156*, 15. https://doi.org/10.1007/s00704-024-05120-w
19. Kirk, B., Amoateng, P., Amponsah, O. (2024). Narrowing down the drivers of flood risk in medium-sized sub-Saharan African cities. *Hydrological Sciences Journal, 69*(13), 1897–1912. https://doi.org/10.1080/02626667.2024.2359946
20. Lafortezza, R., Chen, J., van den Bosch, C. K., Randrup, T. B. (2018). Nature-based solutions for resilient landscapes and cities. *Environmental Research, 165*, 431–441. https://doi.org/10.1016/j.envres.2017.11.038
21. Leulmi, L., Lazri, Y., Abdelkebir, B., Bensehla, S. (2023). Assessment of the effect of LULC change on depth runoff: Case study of Skikda floods event. *Glasnik Srpskog Geografskog Drustva, 103*(2), 145–160. https://doi.org/10.5937/gsgd2302145L
22. Lounis, I., Leulmi, L., Gherzouli, L., Lazri, Y. (2024). Comparative spatio-temporal dynamics of urban sprawl in Algerian cities Skikda and Tébessa (1985–2024). *Journal of Contemporary Urban Affairs, 8*(2), 404–420. https://doi.org/10.30132/JCUA.202481404
23. Lukas, P., Melesse, A. M., Kenea, T. T. (2023). Prediction of future LULC changes using a coupled CA-ANN model in the Upper Omo-Gibe River Basin, Ethiopia. *Remote Sensing, 15*(5), 1148. https://doi.org/10.3390/rs15051148
24. Muhammad, R., Zhang, W., Abbas, Z., Guo, F., Gwiazdzinski, L. (2022). Spatiotemporal change analysis and prediction of future LULC changes using QGIS MOLUSCE plugin. *Land, 11*(3), 419. https://doi.org/10.3390/land11030419
25. Nedelea, A., Stoleriu, C. C., Stoleriu, O. M. (2020). Natural hazards spatial assessment in floodplains. *Applied Sciences, 10*(21), 7560. https://doi.org/10.3390/app10217560
26. Pelling, M., Garschagen, M. (2019). Put equity first in climate adaptation. *Nature, 569*(7756), 327–329. https://doi.org/10.1038/d41586-019-01497-9
27. Reghezza-Zitt, M., Rufat, S. (Eds.). (2015). Résiliences. Sociétés et territoires face à l'incertitude, aux risques et aux catastrophes. *ISTE Éditions / Wiley.* (in French) https://doi.org/10.1002/9781119457107
28. Rentschler, J., Salhab, M., Jafino, B. A. (2022). Flood exposure and poverty in 188 countries. *Nature Communications, 13*, 3527. https://doi.org/10.1038/s41467-022-30727-4
29. Saidi, F. A., Phinzi, K., Molnár, E. (2023). Urbanization in Algeria: Toward a more balanced and sustainable urban network? *Social Sciences, 12*(3), 174. https://doi.org/10.3390/socsci12030174
30. Salhi, A., Larifi, I., Salhi, H., Heggy, E. (2024). Flooding in semi-unformal urban areas in North Africa: Environmental and psychosocial drivers. *Science of the Total Environment, 929*, 172580.
31. Sun, Q., Li, B., Zhang, T., Yuan, Y., Xiao, L. (2022). Multi-scenario urban flood risk assessment by integrating urbanization, climate change and flood modelling. *Natural Hazards and Earth System Sciences, 22*, 3815–3833. https://doi.org/10.5194/nhess-22-3815-2022
32. UNDRR.(2015).SendaiFrameworkforDisasterRiskReduction 2015–2030. https://www.undrr.org/publication/sendai-framework-disaster-risk-reduction-2015-2030
33. UNEP. (2018). The Adaptation Gap Report 2018. https://www.unep.org/resources/adaptation-gap-report-2018
34. Wang, J., Bretz, M., Dewan, M. A. A., Delavar, M. A. (2022). Machine learning in modelling land-use and land cover-change (LULCC). *Science of the Total Environment, 822*, 153559. https://doi.org/10.1016/j.scitotenv.2022.153559
35. Wulder, M. A., Roy, D. P., Radeloff, V. C., Loveland, T. R., Anderson, M. C. (2022). Fifty years of Landsat science and impacts. *Remote Sensing of Environment, 280*, 113195. https://doi.org/10.1016/j.rse.2022.113195